Journal of Molecular Structure 1119 (2016) 385–395

Contents lists available at ScienceDirect

Journal of Molecular Structure

journal homepage: http://www.elsevier.com/locate/molstruc

Synthesis, spectral, structural and computational studies on NiS_4 and NiS_2NP chromophores: Anagostic and C–H···π (chelate) interactions in [Ni(dtc)(PPh_3)(NCS)] (dtc = N-(2-phenylethyl)-N-(4-methoxybenzyl)- dithiocarbamate and N-(2-phenylethyl)-N-(4-chlorobenzyl)dithiocarbamate)

E. Sathiyaraj [a, b], P. Selvaganapathi [a], S. Thirumaran [a, *], Samuele Ciattini [c]

[a] Department of Chemistry, Annamalai University, Annamalinagar 608 002, Tamilnadu, India
[b] Department of Chemistry, Kalasalingam University, Krishnankoil 626 126, India
[c] Centro di Cristallografia Strutturale, Polo Scientifio di Sesto Fiorentino, Via della Lastruccia No. 3, 50019 Sesto Fiorentino, Firenze, Italy

ARTICLE INFO

Article history:
Received 11 December 2015
Received in revised form
12 April 2016
Accepted 25 April 2016
Available online 30 April 2016

Keywords:
Nickel(II)
Dithiocarbamate
Triphenylphosphine
X-ray structure
Anagostic interactions

ABSTRACT

Bis(N-(2-phenylethyl)-N-substituted benzyldithiocarbamato-S,S′)nickel(II) (**1**–**6**) and (N-(2-phenylethyl)-N-substituted benzyldithiocarbamato-S,S′)(thiocyanato-N) (triphenylphosphine)nickel(II) (**7**–**12**) [substituted benzyl = 2HO–C_6H_4–CH_2– **(1,7),** 3HO–C_6H_4–CH_2– **(2,8),** 4HO–C_6H_4–CH_2– **(3,9),** 4CH_3O–C_6H_4–CH_2– **(4,10),** 4F–C_6H_4–CH_2– **(5,11),** 4Cl–C_6H_4–CH_2– **(6,12)**] complexes have been synthesized and characterized by elemental analysis, IR, UV–Vis and NMR (^1H and ^{13}C) spectroscopy. In the case of heteroleptic complexes **7**–**12**, the shift in $\nu_{C\text{-}N}$ values to higher wavenumber and the NCS_2 carbon signals are shifted to downfield compared to the homoleptic complexes indicating the increasing strength of thioureide $\nu_{C\text{-}N}$ bond due to the presence of π-accepting triphenylphosphine ligand in heteroleptic complexes. Electronic spectral studies on all the complexes (**1**–**12**) suggest square planar geometry around the nickel(II). Structures of **10** and **12** have been elucidated by X-ray crystallography. The dithiocarbamate anions in **10** and **12** chelate to the nickel atom. Both the structures reveal C–H···Ni intramolecular anagostic interaction. C–H···π (chelate) is observed in complexes **10**. Supramolecular frame works are stabilised by C–H···S, C–H···π and C–H···Cl non-covalent interaction. The molecular geometry, HOMO-LUMO in the ground state and MEP have been calculated for **10** and **12** using Hartree-Fock (HF) method with LANL2DZ basic set. Molecular electrostatic potential diagram of complexes **10** and **12** support the partial double bond character of C–N (thioureide) bond in dithiocarbamate ligands.

1. Introduction

The importance of coordination chemistry has now become broad and the applications of coordination compounds to the scientific world are tremendous [1]. Several donor atoms like oxygen, sulfur, nitrogen, phosphorous were reported earlier by many pioneer workers in this field. Metal-dithiocarbamate complexes are the most widely studied. Because of the metal binding property and their chelates vital role to biological, agricultural and industrial field etc [2]. Dithiolate Ni(II) complexes, containing a coordination NiS_4 unit, are widely applied in analytical chemistry, organic synthesis and biology. Dithiocarbamate ligands are used to extract metals [3] and their complexes serve as precursors of metal-sulfides in modern electronics [4–11]. Metal dithiocarbamate complexes have numerous applications in the chemical, agricultural and pharmaceutical industry, mainly because of their metal-binding and antioxidant properties [12,13]. A number of bis(dithiocarbamate)nickel(II), [$Ni(dtc)_2$] and [Ni(dtc)(NCS)(PPh_3)] complexes have been synthesized, several of them have been characterized by single crystal X-ray diffraction [14,15]. Non-covalent interactions are fundamental for supramolecular

* Corresponding author.
E-mail address: sthirumaran@yahoo.com (S. Thirumaran).

http://dx.doi.org/10.1016/j.molstruc.2016.04.079
0022-2860/

chemistry, drug design, protein folding, crystal engineering and other areas of molecular science. The crystal engineering of molecules is concerned with intriguing architectures and utilitarian consideration. Non-covalent interactions, such as conventional X–H···Y and non-conventional C–H···X (X or Y = F, Cl, O, N, S) hydrogen bonding, C–H···π, π···π, π(chelate)···π (chelate), π(aryl)···π (chelate), C–H···π (chelate) and X–H···M (X = O, N, C) metal assisted anagostic, agostic and hydrogen bonding interactions, often play crucial roles in the molecular recognition processes and organization of the supramolecular networks [16–30]. Our aim is to study the non-covalent interactions in homoleptic and heteroleptic Ni(II) complexes involving functionalized dithiocarbamate complexes. In this paper, we report the synthesis and characterization of some Ni(II) complexes containing N-(2-phenylethyl)-N-substituted benzyl dithiocarbamates. In addition, Single crystal X-ray structural analysis and computational studies on (N-(2-phenylethyl)-N-4-methoxy benzyldithiocarbamato-S,S′)(thiocyanato-N)(triphenylphosphine)nickel(II) (**10**) and (N-(2-phenylethyl)-N-4-chlorobenzyldithiocarbamato-S,S′)(thiocyanato-N)(triphenylphosphine)nickel(II) (**12**) are also presented.

2. Experimental

2.1. Materials and instrumentation

All reagents and solvents were commercially available high grade materials (Merck/sd Fine/Himedia) and used as received. FT-IR spectra were recorded on a SHIMADZU FT-IR spectrophotometer (range 400–4000 cm^{-1}) as KBr pellets. ^1H NMR spectra were recorded on Bruker 400 MHz and ^{13}C NMR spectra on Bruker 100 MHz in $CDCl_3$ and DMSO-d_6 as a solvent and tetramethylsilane (TMS) as an internal standard. For compounds **1**–**3** dissolved in DMSO-d_6, the two signals of DMSO and water arose at 2.5 and 3.4 ppm, respectively. SHIMADZU UV-1650 PC double beam UV–visible spectrophotometer was used for recording the electronic spectra of the complexes. The spectra were recorded in acetonitrile, chloroform and the pure solvents were used as the reference.

2.2. Syntheses of nickel(II) complexes

2.2.1. Preparation of bis(N-(2-phenylethyl)-N-substituted benzyldithiocarbamato-S,S′)nickel(II)

2-phenylethylamine (4.6 mmol) in methanol was added to substituted benzaldehyde (2-OH, 3-OH, 4-OH, 4-OCH_3, 4-F and 4-Cl) (5.1 mmol) in methanol and the solution was stirred continuously for 2 h. The colourless oil formed on evaporation of the solvent. The product was dissolved in methanol-dichloromethane solvent mixture (1:1, 20 mL) and sodium borohydride (13.8 mmol) was added slowly and stirred continuously for 2 h under ice cold condition (5 °C). Further, the mixture was stirred for 20 h at room temperature. After evaporation of the solvent, the resulting viscous liquid product was washed with water and the product was extracted with dichloromethane. Evaporation of the organic layer yielded N-(2-phenylethyl)-N-substituted benzylamine as pale yellow oil. N-(2-phenylethyl)-N-substituted benzylamine (4 mmol) and carbon disulfide (4.0 mmol) were dissolved in ethanol (20 mL) and stirred for 30 min. Nickel chloride hexahydrate (2.0 mmol) was dissolved in 10 mL of water and added to the solution with constant stirring. The complexes formed were filtered off, dried and recrystallized from acetonitrile (Scheme 1).

2.2.2. Preparation of (N-(2-phenylethyl)-N-substituted benzyldithiocarbamato-S,S′)(thiocyanato-N)(triphenylphosphine) nickel(II)

Bis(N-(2-phenylethyl)-N-substituted benzyldithiocarbamato-S,S′)nickel(II) (1.0 mmol), PPh_3 (2.0 mmol), $NiCl_2 \cdot 6H_2O$ (1.0 mmol) and NH_4SCN (2.0 mmol) were dissolved in chloroform-methanol solvent mixture (3:2, 50 mL) and heated to reflux for 3 h. The solution obtained was filtered off. Purple-red solid formed after 5 days. It was filtered off and recrystallized from chloroform (Scheme 1).

*2.2.2.1. bis(N-(2-phenylethyl)-N-(2-hydroxybenzyl)dithiocarbamato-S,S′)nickel(II) (**1**).* Yield 78%, mp 230–231 °C. IR (KBr, cm^{-1}): ν = 3453 (ν_{OH}); 1510 (ν_{C-N}); 1026 (ν_{C-S}). UV–Vis (CH_3CN, nm): λ = 621, 478, 394, 337, 285, 250. ^1H NMR (400 MHz, DMSO, ppm):δ = 2.83 (b, 4H, (C_6H_5–C**H₂**–CH_2–N)); 3.68 (b, 4H, C_6H_5–CH_2–C**H₂**–N); 4.71 (s, 4H, *2*HO–C_6H_4–C**H₂**–N); 6.83–7.30 (aromatic protons); 9.99 (s, 2H, *2***H**O–C_6H_4–CH_2–N). ^{13}C NMR (100 MHz, DMSO, ppm): δ = 32.5 (C_6H_5–**C**H₂–CH_2–N); 47.4 (C_6H_5–CH_2–**C**H_2–N); 50.4 (*2*HO–C_6H_4–**C**H₂–N); *ipso carbon*; 155.5 (Ar–2OH); 115.3–137.5 (other aromatic carbons); 205.2 (N**C**S_2); Anal. Calcd. for Chemical Formula: $C_{32}H_{32}N_2NiO_2S_4$ (%): Elemental Analysis: C, 57.92; H, 4.86; N, 4.22; Found: C, 57.13; H, 4.61; N, 4.07.

*2.2.2.2. bis(N-(2-phenylethyl)-N-(3-hydroxybenzyl)dithiocarbamato-S,S′)nickel(II) (**2**).* Yield 66%, mp 156–158 °C. IR (KBr, cm^{-1}):ν = 3370 (ν_{OH}); 1501 (ν_{C-N}); 1022 (ν_{C-S}). UV–Vis (CH_3CN, nm): λ = 618, 479, 394, 330, 283, 250. ^1H NMR (400 MHz, DMSO, ppm):δ = 2.84 (b, 4H, (C_6H_5–C**H₂**–CH_2–N)); 3.65 (b, 4H, (C_6H_5–CH_2–C**H₂**–N)); 4.71 (s, 4H,3HO–C_6H_4–C**H₂**–N); 6.74–7.31 (aromatic protons); 9.64 (s, 2H,*3***H**O–C_6H_4–CH_2–N); ^{13}C NMR (100 MHz, DMSO, ppm): δ = 32.4 (C_6H_5–**C**H₂–CH_2–N); 50.2 (C_6H_5–CH_2–**C**H_2–N); 51.8 (*3*HO–C_6H_4–**C**H₂–N); *ipso carbon*;157.7 (Ar–*3*OH); 114.6–137.5 (other aromatic carbons); 205.7 (N**C**S_2); Anal. Calcd. for Chemical Formula: $C_{32}H_{32}N_2NiO_2S_4$ (%): Elemental Analysis: C, 57.92; H, 4.86; N, 4.22; Found: C, 57.94; H, 4.69; N, 4.07.

*2.2.2.3. bis(N-(2-phenylethyl)-N-(4-hydroxybenzyl)dithiocarbamato-S,S′)nickel(II) (**3**).* Yield 75%, mp 176–178 °C. IR (KBr, cm^{-1}): ν = 3360 (ν_{OH}); 1503 (ν_{C-N}); 1020 (ν_{C-S}). UV–Vis (CH_3CN, nm): λ = 618, 478, 435, 393, 313, 275, 252, 246. ^1H NMR (400 MHz, DMSO, ppm):δ = 2.79 (b, 4H, (C_6H_5–C**H₂**–CH_2–N)); 3.61 (b, 4H, (C_6H_5–CH_2–C**H₂**–N)); 4.67 (s, 4H,*4*HO–C_6H_4–C**H₂**–N); 6.79–7.30 (aromatic protons); 9.64 (s, 2H,*4***H**O–C_6H_4–CH_2–N); ^{13}C NMR (100 MHz, $CDCl_3$, ppm): δ = 32.4 (C_6H_5–**C**H₂–CH_2–N); 49.8 (C_6H_5–CH_2–**C**H_2–N); 51.5 (*4*HO–C_6H_4–**C**H₂–N); *ipso carbon*; 157.4 (Ar–*4*OH); 115.4–137.5 (other aromatic carbons); 204.9 (N**C**S_2); Anal. Calcd. for Chemical Formula: $C_{32}H_{32}N_2NiO_2S_4$ (%): Elemental Analysis: C, 57.92; H, 4.86; N, 4.22; Found: C, 57.37; H, 4.87; N, 4.11.

*2.2.2.4. bis(N-(2-phenylethyl)-N-(4-methoxybenzyl)dithiocarbamato-S,S′)nickel(II) (**4**).* Yield 81%, mp 182–184 °C. IR (KBr, cm^{-1}): ν = 1506 (ν_{C-N}); 1022 (ν_{C-S}). UV–Vis ($CHCl_3$, nm): λ = 629, 502, 393, 328, 261. ^1H NMR (400 MHz, $CDCl_3$, ppm):δ = 2.88 (b, 4H, (C_6H_5–C**H₂**–CH_2–N)); 3.65 (b, 4H, (C_6H_5–CH_2–C**H₂**–N)); 3.81 (s, 3H,*4C***H₃**O–C_6H_4–CH_2–N); 4.58 (s, 4H,*4*CH_3O–C_6H_4–C**H₂**–N); 6.87–7.30 (aromatic protons); ^{13}C NMR (100 MHz, $CDCl_3$, ppm): δ = 33.4 (C_6H_5–**C**H₂–CH_2–N); 50.1 (C_6H_5–CH_2–**C**H_2–N); 52.3 (*4*CH_3O–C_6H_4–**C**H₂–N); 55.4 (*4*CH_3O–C_6H_4–**C**H₂–N); *ipso carbon*; 159.7 (Ar–*4*OCH_3); 114.3–137.7 (other aromatic carbons); 207.9 (N**C**S_2); Anal. Calcd. for Chemical Formula: $C_{34}H_{36}N_2NiO_2S_4$ (%): Elemental Analysis: C, 59.04; H, 5.25; N, 4.05; Found: C, 58.46; H, 4.99; N, 4.00.

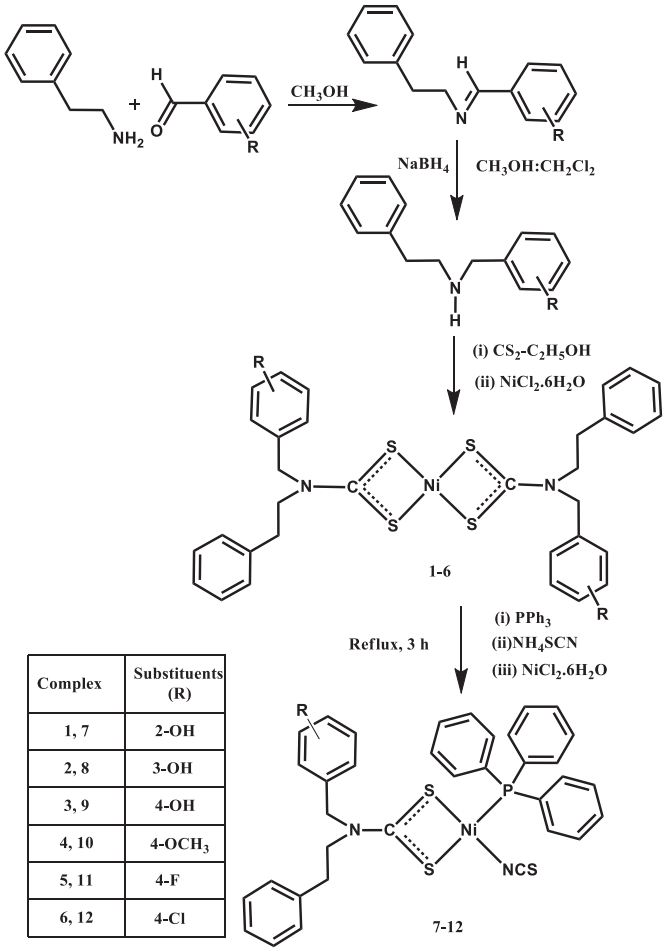

Complex	Substituents (R)
1, 7	2-OH
2, 8	3-OH
3, 9	4-OH
4, 10	4-OCH_3
5, 11	4-F
6, 12	4-Cl

Scheme 1. Preparation of homoleptic and heteroleptic nickel(II) complexes **1**–**12**.

*2.2.2.5. bis(N-(2-phenylethyl)-N-(4-fluorobenzyl)dithiocarbamato-S,S′)nickel(II) (**5**).* Yield 77%, mp 178–180 °C. IR (KBr, cm^{-1}): $\nu = 1504$ (ν_{C-N}); 1020 (ν_{C-S}). UV–Vis ($CHCl_3$, nm): $\lambda = 637, 498, 394, 328, 263$. ^1H NMR (400 MHz, $CDCl_3$, ppm):$\delta = 2.91$(b, 4H, (C_6H_5–C***H*****2**–CH_2–N)); 3.67 (b, 4H, (C_6H_5–CH_2–C***H*****2**–N)); 4.59 (s, 4H,4F–C_6H_4–C***H*****2**–N); 7.03–7.31 (aromatic protons); ^{13}C NMR (100 MHz, $CDCl_3$, ppm): $\delta = 33.4$ (C_6H_5–***C*****H2**–CH_2–N); 50.3 (C_6H_5–CH_2–***C*****H2**–N); 52.0 (*4*F–C_6H_4–***C*****H2**–N); *ipso carbon*; 161.5, 163.9 (Ar-*4*F); 115.9–137.6 (other aromatic carbons); 208.6 (N***C***S_2); Anal. Calcd. for Chemical Formula: $C_{32}H_{30}F_2N_2NiS_4$ (%): Elemental Analysis: C, 57.58; H, 4.53; N, 4.20; Found: C, 57.08; H, 4.23; N, 4.10.

*2.2.2.6. bis(N-(2-phenylethyl)-N-(4-chlorobenzyl)dithiocarbamato-S,S′)nickel(II) (**6**).* Yield 78%, mp 196–198 °C. IR (KBr, cm^{-1}): $\nu = 1499$ (ν_{C-N}); 1020 (ν_{C-S}). UV–Vis ($CHCl_3$, nm): $\lambda = 631, 498, 393, 329, 265$. ^1H NMR (400 MHz, $CDCl_3$, ppm):$\delta = 2.91$(b, 4H, (C_6H_5–C***H*****2**–CH_2–N)); 3.67 (b, 4H, (C_6H_5–CH_2–C***H*****2**–N)); 4.58 (s, 4H,*4*Cl–C_6H_4–C***H*****2**–N); 7.17–7.34 (aromatic protons); ^{13}C NMR (100 MHz, $CDCl_3$, ppm): $\delta = 33.4$ (C_6H_5–***C*****H2**–CH_2–N); 50.4 (C_6H_5–CH_2–***C*****H2**–N); 52.1 (*4*Cl–C_6H_4–***C*****H2**–N); 127.0–137.5 (aromatic carbons); 208.9 (N***C***S_2): Anal. Calcd. for Chemical Formula: $C_{32}H_{30}Cl_2N_2NiS_4$ (%): Elemental Analysis: C, 54.87; H, 4.32; N, 4.00; Found: C, 54.51; H, 4.18; N, 4.03.

*2.2.2.7. (N-(2-phenylethyl)-N-(2-hydroxybenzyl)dithiocarbamato-S,S′)(thiocyanato-N) (triphenylphosphine)nickel(II) (**7**).* Yield 80%, mp 180–182 °C. IR (KBr, cm^{-1}): $\nu = 3240$ (ν_{OH}); 1520 (ν_{C-N}); 2099 (ν_{NCS}); 1024 (ν_{C-S}). UV–Vis (CH_3CN, nm): $\lambda = 483, 331, 274, 257$. ^1H NMR (400 MHz, DMSO, ppm): $\delta = 2.69, 2.81$ (bd, 4H, (C_6H_5–C***H*****2**–CH_2–N)); 3.49, 3.65 (bd, 4H, (C_6H_5–CH_2–C***H*****2**–N)); 4.56, 4.75 (bd, 4H, *2*HO–C_6H_4–C***H*****2**–N); 6.86–7.71 (aromatic protons); ^{13}C NMR (100 MHz, $CDCl_3$, ppm): $\delta = 33.4$ (C_6H_5–***C*****H2**–CH_2–N); 47.5 (C_6H_5–CH_2–***C*****H2**–N); 50.9 (*2*HO–C_6H_4–***C*****H2**–N); *ipso carbon*; 154.9 (Ar–*2*OH); 116.1–137.3 (other aromatic carbons); 143.2(N***C***S); 203.6 (N***C***S_2); Anal. Calcd. for Chemical Formula: $C_{35}H_{31}N_2NiOPS_3$ (%): Elemental Analysis: C, 61.68; H, 4.58; N, 4.11; Found: C, 61.32; H, 4.50; N, 3.99.

*2.2.2.8. (N-(2-phenylethyl)-N-(3-hydroxybenzyl)dithiocarbamato-S,S′)(thiocyanato-N) (triphenylphosphine)nickel(II) (**8**).* Yield 78%, mp 151–153 °C. IR (KBr, cm^{-1}): $\nu = 3323$ (ν_{OH}); 2097 (ν_{C-N}); 1518 (ν_{C-N}); 1022 (ν_{C-S}). UV–Vis (CH_3CN, nm): $\lambda = 484, 332, 260$. ^1H NMR (400 MHz, DMSO, ppm):$\delta = 2.71, 2.81$ (bd, 4H, (C_6H_5–C***H*****2**–CH_2–N)); 3.46, 3.64 (bd, 4H, (C_6H_5–CH_2–C***H*****2**–N)); 4.36,4.57 (bd, 4H, *3*HO–C_6H_4–C***H*****2**–N); 6.61–7.73 (aromatic protons); ^{13}C NMR (100 MHz, $CDCl_3$, ppm): $\delta = 33.4$ (C_6H_5–***C*****H2**–CH_2–N); 50.4 (C_6H_5–CH_2–***C*****H2**–N); 52.6 (*3*HO–C_6H_4–***C*****H2**–N); *ipso carbon*;156.8 (Ar–*3*OH); 115.6–137.1 (other aromatic carbons); 143.5 (N***C***S); 204.7 (N***C***S_2); Anal. Calcd. for Chemical Formula: $C_{35}H_{31}N_2NiOPS_3$ (%): Elemental Analysis: C, 61.68; H, 4.58; N, 4.11; Found: C, 61.25; H, 4.62; N, 3.92.

*2.2.2.9. (N-(2-phenylethyl)-N-(4-hydroxybenzyl)dithiocarbamato-S,S′)(thiocyanato-N) (triphenylphosphine)nickel(II) (**9**).* Yield 74%, mp 194–196 °C. IR (KBr, cm^{-1}): $\nu = 3248$ (ν_{OH}); 2100 (ν_{NCS}); 1512 (ν_{C-N}); 1015 (ν_{C-S}). UV–Vis (CH_3CN, nm): $\lambda = 482, 333, 273, 254$. ^1H NMR (400 MHz, DMSO, ppm):$\delta = 2.67, 2.81$ (bd, 4H, (C_6H_5–C***H*****2**–CH_2–N)); 3.43, 3.60 (bd, 4H, (C_6H_5–CH_2–C***H*****2**–N)); 4.34, 4.55 (bd, 4H, *4*HO–C_6H_4–C***H*****2**–N); 6.82–7.64 (aromatic protons); ^{13}C NMR (100 MHz, DMSO, ppm): $\delta = 33.4$ (C_6H_5–***C*****H2**–CH_2–N); 50.1 (C_6H_5–CH_2–***C*****H2**–N); 52.3 (*4*HO–C_6H_4–***C*****H2**–N); *ipso carbon*;156.2 (Ar–*4*OH); 116.0–137.2 (other aromatic carbons); 204.5 (N***C***S_2); Anal. Calcd. for Chemical Formula: $C_{35}H_{31}N_2NiOPS_3$ (%): Elemental Analysis: C, 61.68; H, 4.58; N, 4.11; Found: C, 61.33; H, 4.39; N, 4.01.

*2.2.2.10. (N-(2-phenylethyl)-N-(4-methoxybenzyl)dithiocarbamato-S,S′)(thiocyanato-N) (triphenylphosphine)nickel(II) (**10**).* Yield 76%, mp 186–187 °C. IR (KBr, cm^{-1}): $\nu = 2091$ (ν_{NCS}); 1514 (ν_{C-N}); 1026 (ν_{C-S}). UV–Vis ($CHCl_3$, nm): $\lambda = 483, 329, 260$. ^1H NMR (400 MHz, $CDCl_3$, ppm):$\delta = 2.67, 2.83$ (bd, 4H, (C_6H_5–C***H*****2**–CH_2–N)); 3.44, 3.62 (bd, 4H, (C_6H_5–CH_2–C***H*****2**–N)); 3.80 (s, 3H, *4*C***H*****3**O–C_6H_4–CH_2–N); 4.37, 4.57 (bd, 4H, *4*CH_3O–C_6H_4–C***H*****2**–N); 6.86–7.74 (aromatic protons); ^{13}C NMR (100 MHz, $CDCl_3$, ppm): $\delta = 33.5$ (C_6H_5–***C*****H2**–CH_2–N); 50.1 (C_6H_5–CH_2–***C*****H2**–N); 52.3 (*4*CH_3O–C_6H_4–***C*****H2**–N); 55.4 (*4*C***H*****3**O–C_6H_4–CH_2–N); *ipso carbon*; 159.9 (Ar–*4*OCH_3); 114.5–137.2 (other aromatic carbons); 204.2 (N***C***S_2); Anal. Calcd. for Chemical Formula: $C_{36}H_{33}N_2NiOPS_3$ (%): Elemental Analysis: C, 62.17; H, 4.78; N, 4.03; Found: C, 61.88; H, 4.60; N, 3.84.

*2.2.2.11. (N-(2-phenylethyl)-N-(4-fluorobenzyl)dithiocarbamato-S,S′)(thiocyanato-N) (triphenylphosphine)nickel(II) (**11**).* Yield 79%, mp 169–171 °C. IR (KBr, cm^{-1}): $\nu = 2089$ (ν_{NCS}); 1510 (ν_{C-N}); 1018 (ν_{C-S}). UV–Vis ($CHCl_3$, nm): $\lambda = 487, 332, 253$. ^1H NMR (400 MHz, $CDCl_3$, ppm):$\delta = 2.78$ (b, 4H, (C_6H_5–C***H*****2**–CH_2–N)); 3.51 (b, 4H, (C_6H_5–CH_2–C***H*****2**–N)); 4.50 (b, 4H,4F–C_6H_4–C***H*****2**–N); 7.04–7.71 (aromatic protons); ^{13}C NMR (100 MHz, $CDCl_3$, ppm): $\delta = 33.5$ (C_6H_5–***C*****H2**–CH_2–N); 50.3 (C_6H_5–CH_2–***C*****H2**–N); 52.3

(*4*F–C_6H_4–***C*H*2***–N); *ipso carbon*; 161.5, 164.0 (Ar-*4*F); 116.0–137.1 (other aromatic carbons); 205.2 (N***C***S_2); Anal. Calcd. for Chemical Formula: $C_{35}H_{30}FN_2NiPS_3$ (%): Elemental Analysis: C, 61.50; H, 4.22; N, 4.10; Found: C, 61.09; H, 4.06; N, 3.86.

*2.2.2.12. (N-(2-phenylethyl)-N-(4-chlorobenzyl)dithiocarbamato-S,S′)(thiocyanato-N) (triphenylphosphine)nickel(II) (**12**).* Yield 78%, mp 164–166 °C. IR (KBr, cm^{-1}): $\nu = 2089$ (ν_{NCS}); 1514 (ν_{C-N}); 1022 (ν_{C-S}). UV–Vis ($CHCl_3$, nm): $\lambda = 485, 335, 259$. ^{1}H NMR (400 MHz, $CDCl_3$, ppm):δ = 2.71, 2.86, (bd, 4H, (C_6H_5–C***H*2***–CH_2–N)); 3.45, 3.64 (bd, 4H, (C_6H_5–CH_2–C***H*2***–N)); 4.37, 4.59 (bd, 4H, *4*Cl–C_6H_4–C***H*2***–N); 6.99–7.73 (aromatic protons); ^{13}C NMR (100 MHz, $CDCl_3$, ppm): δ = 33.4 (C_6H_5–***C*H*2***–CH_2–N); 50.4 (C_6H_5–CH_2–***C*H*2***–N); 52.3, 51.9 (*4*Cl–C_6H_4–***C*H*2***–N); 127.2–137.0 (aromatic carbons); 144.0 (N***C***S); 205.7 (N***C***S_2); Anal. Calcd. for Chemical Formula: $C_{35}H_{30}ClN_2NiPS_3$ (%): Elemental Analysis: C, 60.06; H, 4.32; N, 4.00; Found: C, 59.80; H, 4.11; N, 3.88.

2.3. X-ray diffraction analysis

Intensity data for the crystals of **10** and **12** were collected on an Xcalibur Sapphire3 with CCD diffractometer instrument, using graphite monochromated MoKα radiation (λ = 0.71073 Å). Cell parameters were determined by least-squares refinement of the diffraction data. The structures were solved with direct methods with SHELXS97 [31] and refined by full-matrix least squares procedures on F^2 with SHELXL97 [32]. All the non-hydrogen atoms were refined anisotropically and the hydrogen atoms were refined isotropically.

3. Results and discussion

3.1. Infrared spectral studies

In the IR spectra of metal-dithiocarbamate complexes, the bands due to the ν_{C-N} and ν_{C-S} stretching modes are important. In the case of dithiocarbamates, ν_{C-N} appears usually in the region 1450–1550 cm^{-1}, an intermediate value between those of a typical single and double bonded C–N bonds. In the present study, IR spectra of complexes **1**–**12** reveal a band in the region 1499–1520 cm^{-1} assigned to the ν_{C-N} vibration [33]. This band is characteristic of N–C(S_2) bond with an intermediate bond order between a single and double bond. The bands in the region 950–1050 cm^{-1} are diagnostic in deciding the coordination mode (monodentate or bidentate) of dithiocarbamate [34]. In this investigation, a single band is observed in the region 1015–1026 cm^{-1}. This confirms that the coordination of the bisN-(2-phenylethyl)-N-substituted benzyldithiocarbamate ligands to the nickel atom corresponds to a bidentate mode. The observed stretching frequency around 2090 cm^{-1} for heteroleptic complexes **7**–**12** is attributed to the N-coordinated thiocyanate [35–39]. The O–H stretching vibrations appear around 3240–3253 cm^{-1} in the complexes **1**–**3** and **7**–**9**.

3.2. Electronic spectral studies

The bands appear in the UV region of electronic spectra of homoleptic and heteroleptic complexes **1**–**12** are ascribed to the intramolecular intraligand transitions corresponding to $\pi \rightarrow \pi^*$ transitions of the N–C═S, S–C═S groups and $n \rightarrow \pi^*$ transition located on the sulfur atom [40,41]. The electronic spectra of the complexes (**1**–**6**) show two weak *d*–*d* bands around 480 and 620 nm. These bands can be assigned to the $d_z^2 \rightarrow d_{x-y}^{22}$ (*ca.* 480 nm) and $d_{xy} \rightarrow d_{x-y}^{22}$ (*ca.* 620 nm) transitions. Bands observed around 480 nm for complexes (**7**–**12**) can be attributed to $d_z^2/d_{xy} \rightarrow d_{x-y}^{22}$ transitions. These d–d transitions in homoleptic and heteroleptic complexes (**1**–**12**) indicate that the geometry in the vicinity of the nickel atom is probably square planar [42].

3.3. NMR spectral studies

3.3.1. ^{1}H NMR spectral studies

For all the complexes **1**–**12**, a singlet or two broad signals observed in the region 4.30–4.75 ppm are assigned to the methylene protons of substituted benzyl group. All the complexes show two sets of signals in the region 3.40–3.68 and 2.67–2.91 ppm associated with methylene protons of ethyl group of phenylethyl; that bound to nitrogen appearing at relatively lowfield. The signals due to the methylene protons adjacent to nitrogen atom are deshielded on complexation. The other proton signals are not greatly affected in all the complexes because of the relative distance from the thioureide π-system [43].

Each methylene protons of dithiocarbamate in heteroleptic complexes **7**–**12** are appeared as a broad or two broad signals due to the fast isothiocyanate ligand exchange process as observed in [Ni(dtc)(PPh_3)(NCS)] [44]. In the complexes **1**–**3,** a singlet observed in the downfield around 10.0 ppm is assigned to the hydroxyl proton. $CDCl_3$ was used as a solvent to record ^{1}H NMR spectra of complexes **7**–**9**. In these cases, the OH proton signal merged with the aromatic proton signals. A singlet observed at 3.80 ppm in complexes **4** and **10** is due to the methoxy methyl protons. In the aromatic region, a triplet at 7.05 ppm and a broad signal at 7.04 ppm are observed for complexes **5** and **11**, respectively. These signals correspond to the protons ortho to fluorine atom. Apart from these signals, signals observed in the region 6.61–7.73 ppm are due to the phenyl ring protons.

3.3.2. ^{13}C NMR spectral studies

Complexes **1**–**12** exhibit three signals in the aliphatic region associated with the methylene carbons of dithiocarbamates. The signal for methylene carbon of benzyl group appears around 50.0 ppm. The remaining two signals in the aliphatic region are due to the methylene carbons of ethylene unit of phenylethyl group of dithiocarbamate that bound nitrogen atom appearing at relatively highfield. Phenyl ring carbons of dithiocarbamate ligands and triphenylphosphine are observed in the region 114.0–164.0 ppm.

^{13}C NMR signals of the dithiocarbamate carbons (NCS_2) appear from 203.0 to 209.0 ppm for complexes **1**–**12**. The upfield shift of NCS_2 carbon signals for heteroleptic complexes **10**–**12** (204.5–205.7 ppm) compared to the homoleptic complexes **4**–**6** (207.9–208.9 ppm) is ascribed to increase of π-bond character. This is due to the presence of π-acid (triphenylphosphine) in heteroleptic complexes which increases the mesomeric drift of electron density from the dithiocarbamate moiety towards the metal atom [45]. Comparison of the NCS_2 chemical shifts of heteroleptic complexes **7**–**9** with homoleptic complexes **1**–**3** is not possible because the ^{13}C NMR spectra of these complexes were recorded in different solvents.

A very weak signal observed around 143.0 ppm for complexes **7**, **8** and **12** are assigned to the carbon of thiocyanate. A signal in the downfield region 154.9–159.9 ppm for complexes **1**–**4** and **7**–**10** are assigned to ipso carbon of the OH and methoxy function in the phenyl ring. ^{13}C NMR spectra of the complexes **5** and **11** show two signal around 161.0 and 164.0 ppm due to the *ipso* carbon.

Table 1
Crystal data, data collection and refinement parameters for **10** and **12**.

	10	12
Empirical formula	C_{36} H_{33} N_2 Ni O P S_3	C_{35} H_{30} Cl N_2 Ni P S_3
FW	695.50	699.92
Crystal dimensions (mm)	0.35 × 0.30 × 0.20	0.5 × 0.4 × 0.3
Crystal system	Monoclinic	monoclinic
Space group	P 21/n	P21/n
a/Å	10.087(1)	9.820(1)
b/Å	20.104(1)	20.399(1)
c/Å	17.551(1)	17.425(1)
α/°	90.00	90.00
β/°	104.72(1)	102.877(3)
γ/°	90.00	90.00
V/Å^3	3442.3(4)	3402.8(4)
Z	4	4
Dc/g cm^{-3}	1.342	1.366
μ/cm^{-1}	0.823	0.907
F(000)	1448	1448
λ/Å	MoK$_\alpha$ (0.71073)	MoK$_\alpha$ (0.7107)
ange/°	4.13–29.03	4.25–29.23
Index ranges	$-13 \le h \le 13$, $-26 \le k \le 25$, $-23 \le l \le 22$	$-11 \le h \le 13$, $-25 \le k \le 26$, $-23 \le l \le 22$
Reflections collected	23663	23005
Observed reflections I > 2σ(I)	4592	8022, 5005
Weighting scheme	Calc. $W = 1/(\sigma^2(F_o^2) + (0.0477p)^2 + 0.7371p)$ where $p = (F_o^2 + 2F_c^2)/3$	Calc. $W = 1/(\sigma^2(F_o^2) + (0.0544p)^2 + 0.6468p)$ where $p = (F_o^2 + 2F_c^2)/3$
Number of parameters refined	352	388
R[$F^2 > 2\sigma(F^2)$], wR(F^2)	0.0315, 0.0827	0.0541, 0.1180
GOOF	0.957	1.030

3.4. Single crystal X-ray structural analysis

3.4.1. Structural analysis of complexes 10 and 12

Details of the crystal data, data collection and refinement parameters for **10** and **12** are summarized in Table 1. Single crystals of **10** and **12** were obtained by the slow evaporation of dichloromethane: acetonitrile and chloroform: acetonitrile solution, respectively. The intensity data were collected at 150(2) K for **10** and 293(2) K for **12**. The ORTEP diagrams are shown in Figs. **1** and **2**. Selected bond distances and angles are given in Table 2.

In both the complexes **10** and **12,** the nickel cation is coordinated by two sulfur atoms from dithiocarbamate ligands, one nitrogen atom from thiocyanate and one phosphorus atom from PPh_3 into a distorted square planar configuration. The angles S1–Ni–P1, N2–Ni–P1 and N2–Ni–S2 are less distorted from 90° than the angle S1–Ni–S2. The S1–Ni–S2 angle is smaller than 90° due to the chelation of dithiocarbamate ligand. The structure consists of distorted square planar metal coordination with NiS_2PN chromophore. Based on the value of τ_4 (0.07), the coordination geometries of **10** and **12** are described as being 7% along the pathway of distortion from perfect square planar to seesaw structure [46]. The Ni–S bond distances [Ni–S1 = 2.2291(9) and Ni–S2 = 2.1634(9) Å] for **10** and [Ni–S1 = 2.1702(10) and Ni–S2 = 2.2245(9) Å] for **12** are significantly different. The Ni–S bond *trans* to PPh_3 is longer than the other Ni–S bond. This is owing to the greater *trans* effect of triphenylphosphine compared to those of the NCS^- [35–39]. The average C–S bond lengths [1.721(3) and 1.715 (3) for **10** and **12**, respectively] and C–N bond length [1.312(4) and 1.318(4) Å for **10** and **12**, respectively] are in the range those established for the C–S partial double bond and C–N (thioureide) bond in dithiocarbamates [47].

The Ni–N distances [1.866(3) and 1.860(3) Å for **10** and **12,** respectively] are quite short, showing the effective bonding between the nickel atom and the thiocyanate-N. The C–S bond lengths in thiocyanate is 1.617(4) and 1.620(4) Å for **10** and **12**,

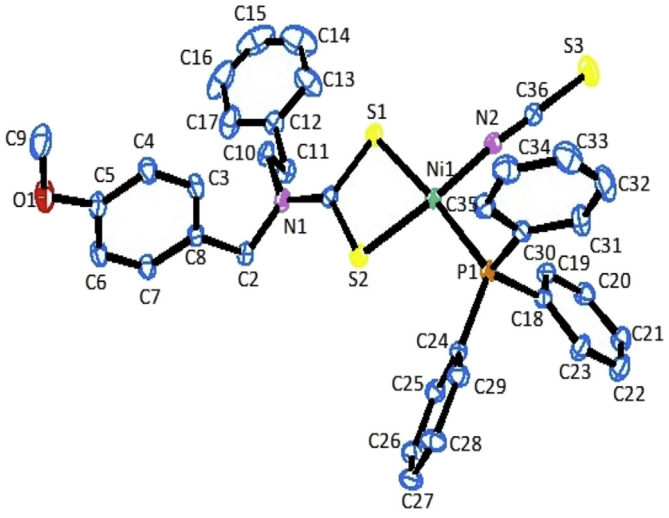

Fig. 1. ORTEP diagram of complex **10.**

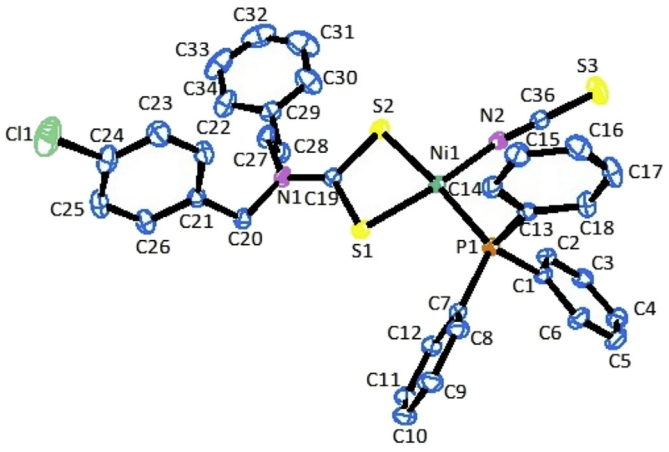

Fig. 2. ORTEP diagram of complex **12.**

Table 2
Selected bond distances (Å) and angles (°) for complexes **10** and **12**.

10		12	
Bond distances (Å)		Bond distances (Å)	
Ni1–N2	1.866(3)	Ni1–N2	1.860(3)
Ni1–S2	2.1634(9)	Ni1–S1	2.1702(10)
Ni1–P1	2.1871(9)	Ni1–P1	2.1903(8)
Ni1–S1	2.2291(9)	Ni1–S2	2.2245(9)
S2–C1	1.726(3)	S1–C19	1.722(3)
S1–C1	1.715(3)	S2–C19	1.708(3)
S3–C36	1.617(4)	S3–C36	1.620(4)
C36–N2	1.150(4)	C19–N1	1.318(4)
N1–C1	1.312(4)	C36–N2	1.150(4)
Bond angles (°)		Bond angles (°)	
N2–Ni1–S2	174.86(8)	N2–Ni1–S1	174.62(8)
N2–Ni1–P1	88.99(8)	N2–Ni1–P1	88.89(8)
S2–Ni1–P1	95.95(3)	S1–Ni1–P1	96.28(3)
N2–Ni1–S1	95.99(8)	N2–Ni1–S2	95.98(8)
S2–Ni1–S1	79.11(3)	S1–Ni1–S2	
P1–Ni1–S1	174.77(4)	P1–Ni1–S2	174.96(4)
C1–S2–Ni1	86.67(11)	C19–S1–Ni1	86.66(12)
C1–S1–Ni1	84.87(11)	C19–S2–Ni1	85.29(11)
N2–C36–S3	178.3(3)	N1–C19–S2	125.8(2)
N1–C1–S1	125.6(2)	N1–C19–S1	125.2(3)
N1–C1–S2	125.6(3)	S2–C19–S1	109.00(18)
S1–C1–S2	108.82(18)	N2–C36–S3	179.0(3)
C36–N2–Ni1	172.3(3)	C36–N2–Ni1	171.0(3)

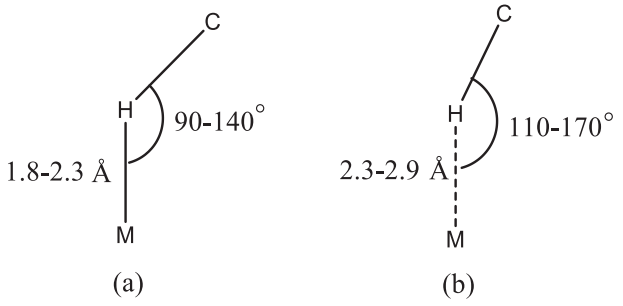

Scheme 2. Geometric difference between (a) agostic and (b) anagostic interaction.

respectively which is similar to the C═S distance of 1.69 Å. The Ni–P distance is similar to those found in other [Ni(dtc)(NCS)(PPh_3)] complexes [35–39].

Three types C–H···M interactions observed in transition metal

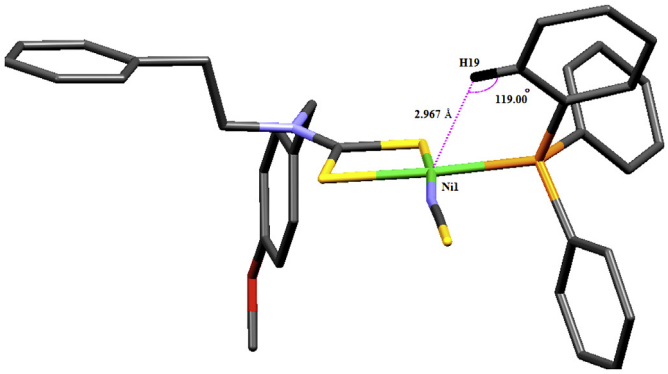

Fig. 3. Intramolecular C–H···Ni anagostic interaction in complex **10.**

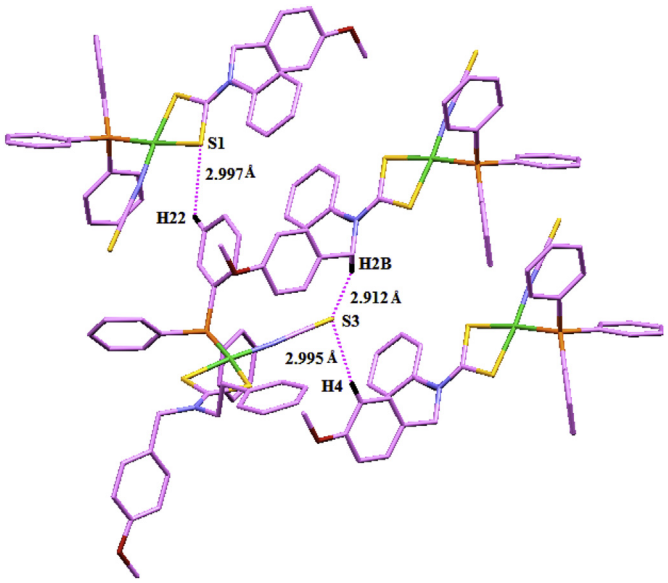

Fig. 4. Intermolecular S···H–C interactions in complex **10**.

Table 3
Geometric details of hydrogen bonding (Å,°) in complex **10**.

Interactions	D–H	H···A	D···A	D–H···A
C19–H19···Ni1[a]	0.93	2.967	3.512(3)	119.00
C2–H2A···S2[b]	0.97	2.565	3.095(4)	114.40
C10–H10A···S1[b]	0.97	2.677	3.072(4)	104.36
C22–H22···S1[c]	0.93	2.997	3.714(4)	135.11
C2–H2B···S3[c]	0.93	2.912	3.857(4)	165.15
C4–H4···S3[c]	0.93	2.995	3.919(4)	172.26

[a] Intramolecular anagostic interaction.
[b] Intramolecular hydrogen bonding.
[c] Intermolecular hydrogen bonding.

complexes are (i). agostic (ii). anagostic or preagostic (Scheme 2) and (iii) hydrogen bonding. Agostic interactions are 3c–2e bonding interactions with <M···H–C angles in the range ~90–140° and M···H distances in the range ~1.8–2.3 Å. Anagostic interactions are somewhat weaker than agostic interaction. They

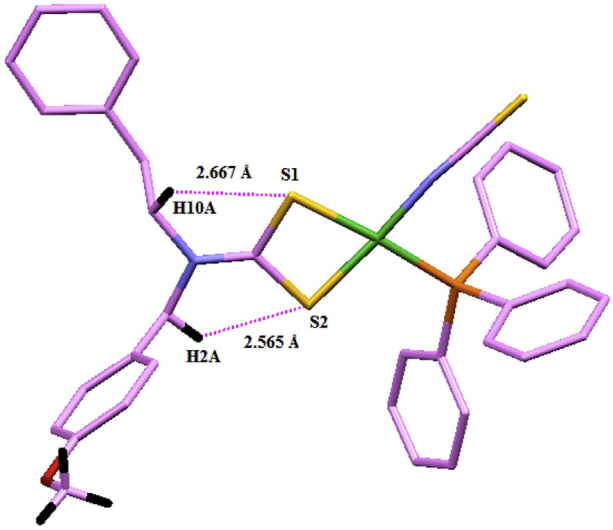

Fig. 5. Intramolecular S···H–C interactions in complex **10.**

are characterized by long M···H distance (~2.3–2.9 Å) and <M···H–C angles in the range ~110–170°. Hydrogen bonds are 3c–4e interactions with almost linear geometry [48]. In complex **10**, it is particularly interesting that packing effects, steric and electronic effects of dithiocarbamate and triphenylphosphine ligands and square planar Ni(II), d^8 force the ortho proton of a phenyl ring in triphenylphosphine ligand to be close proximity to an axial position around the nickel atom thus creating weak anagostic interaction [Ni···H = 2.967 Å and <C–H···Ni = 119°] (Fig. 3). The complexes with anagostic interactions are believed to act as catalysts. S1 of CS_2 and S3 of thiocyanate form intermolecular C–H···S bond with H22 and H4 of phenyl rings, respectively (Fig. 4). S1 and S2 of CS_2 group are involved in the formation of intramolecular C–H···S bonds with H10A and H2A of methylene groups, respectively (Table 3, Fig. 5).

A weak C–H···Ni intramolecular anagostic interaction is also observed in complex **12** (Fig. 6, Table 4). Recently, Tiekink and Zukerman-Schpector have reported [16] that C–H···π (chelate ring) interactions play an important role in stabilizing crystal structures of metal bis(1,1-dithiolates). C–H···Cg (chelate) interactions lead to the formation of 1D, 2D and 3D supramolecular assemblies (Scheme 3). The C–H···Cg (chelate) interaction parameters are defined as d_1, the distance between the ring centroid of the MS_2C ring and the H atom (2.4–3.6 Å), α, angle between the perpendicular to the MS_2C ring (α < 20°) and d_1, and β, the C–H···Cg angle (β = 110–180°). In complex **12**, NiS_2C ring involves the C–H···π (chelate) interaction. The dimension of C–H···π (chelate) interaction is α = 16°, β = 149° and d = 3.605 Å (Fig. 7). Complex **12** is stabilized by C–H···π intermolecular interaction with H16···Cg2 (Centroid of C13–C18 phenyl ring) distance of 3.016 Å which gives rise to chain structure in solid state (Fig. 8). Intermolecular C–H···Cl (H10···Cl1 = 2.897 Å) interaction is also observed (Fig. 9). S1 and S2 involve in the formation of intramolecular C–H···S interactions [C20–H20A···S1 = 2.575 and C27–H27A···S2 = 2.674 Å]. Sulfur of thiocyanate (S3) forms intermolecular C–H···S bonds with H20B and H23B [C20–H20B···S3 = 2.853 and C23–H23···S3 = 2.801 Å] (Fig. 10).

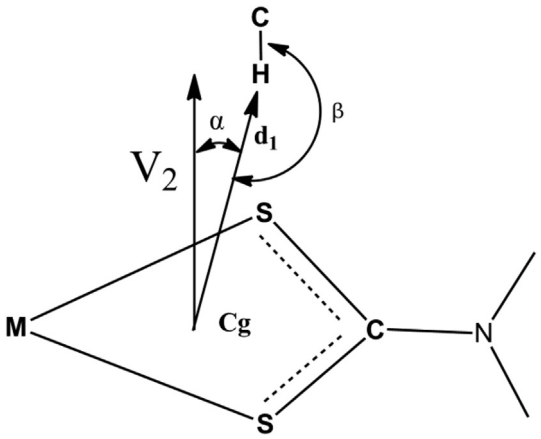

Scheme 3. The parameters for C–H···Cg (chelate) interactions: d1 = 2.4–3.6 Å, α < 20° and β = 110–180°.

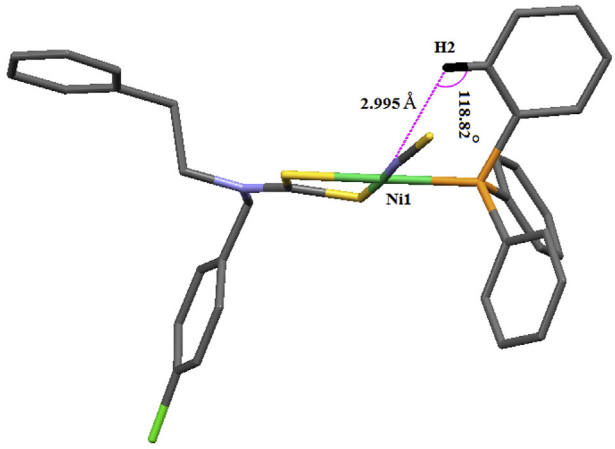

Fig. 6. Intramolecular C–H···Ni anagostic interaction in complex **12.**

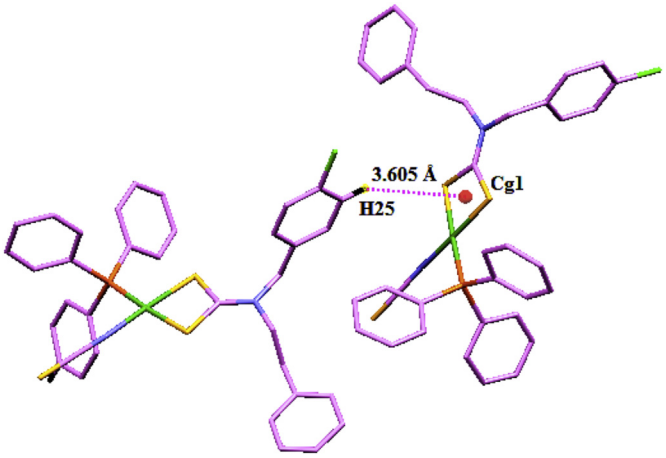

Fig. 7. Intermolecular C–H···π (chelate) interaction in complex **12.**

Table 4
Geometric details of hydrogen bonding (Å,°) in complex **12**.

Interactions	D–H	H···A	D···A	D–H···A
C2–H2···Ni[a]	0.93	2.995	3.538(3)	118.82
C25–H25···Cg1[b] [C19,S2,S1,Ni]	0.93	3.605	4.428(4)	148.96
C16–H16···Cg2[C] [C13–C18]	0.93	3.016	3.906(4)	160.79
C10–H10···Cl1[d]	0.93	2.897	3.664(5)	140.45
C23–H23···S3[d]	0.93	2.801	3.728(5)	175.30
C20–H20B···S3[d]	0.97	2.853	3.792(4)	163.19
C27–H27A···S2[e]	0.97	2.674	3.069(4)	104.81
C20–H20A···S1[e]	0.97	2.575	3.104(4)	114.36

[a] Intramolecular anagostic interaction.
[b] C–H···π (chelate) interaction.
[c] Intermolecular C–H···π interaction.
[d] Intermolecular C–H···Cl and C–H···S interactions.
[e] Intramolecular C–H···S interaction.

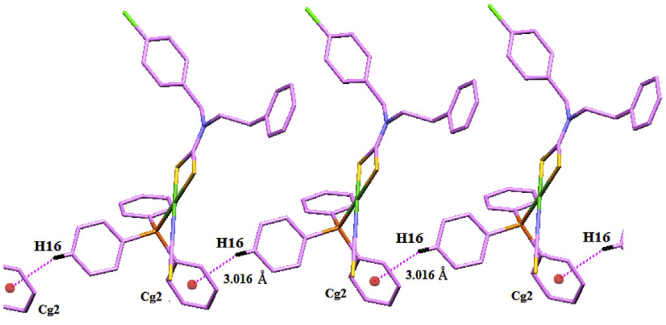

Fig. 8. Molecular chain through intermolecular C–H···π interaction in complex **12.**

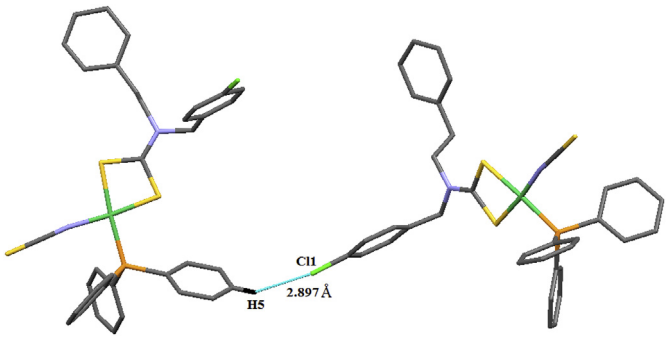

Fig. 9. Intermolecular C–H···Cl interaction in complex **12.**

3.4.2. Theoretical calculations

All calculations were performed with GAUSSIAN09 program package [49] with the aid of the Gauss View visualization program. The optimized structure of complexes **10** and **12** was given in Figs. 11 and 12. The theoretical and experimental values for the selected bond lengths and angles are given in Table 5. The parameters of interest are Ni–S, Ni–N, Ni–P, C–S and C–N bond distances and associated angles. Comparison of the experimental bond parameters with the calculated values of both the complexes shows that the bond length difference is in the range 0.001–0.072 Å for Ni–N, C–S, C–N (thioureide), C–N (NCS) and C–S (thiocyanate) and the bond angle difference is in the range for 0.03–0.75° for N–Ni–P, N–Ni–S1 and C–S1–Ni. The anagostic interaction observed in experimental structural analysis is not found in optimized structures [Calculated values: C–H···Ni = 3.2014 and 3.1939 Å for **10** and **12,** respectively]. This indicates that the packing effects in solid state force the ortho proton of phenyl ring in triphenylphosphine to create anagostic interaction. These differences between experimental and theoretical values are due to the following reasons; all of the calculated data are for the molecule in gas phase and these are no inter- and intramolecular interactions while the experimental data are for the molecule in solid state and there are molecular interactions among them.

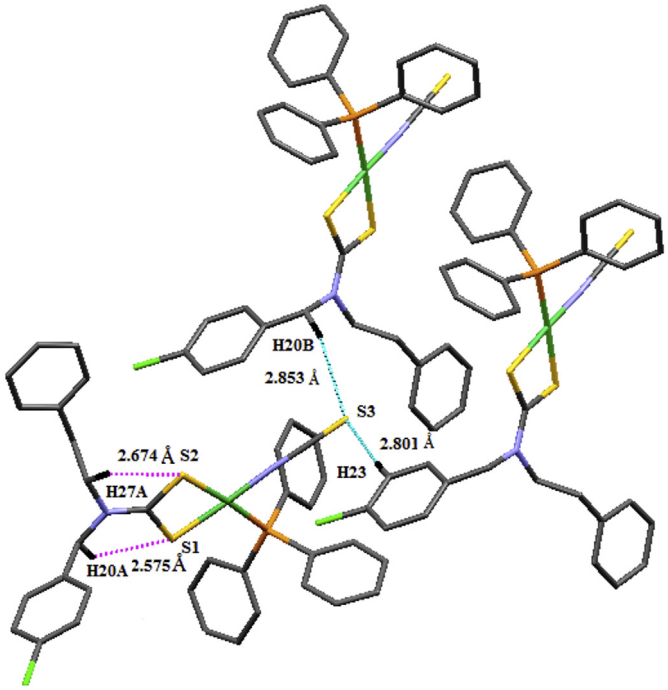

Fig. 10. Intra- and intermolecular C–H···S interactions in complex **12.**

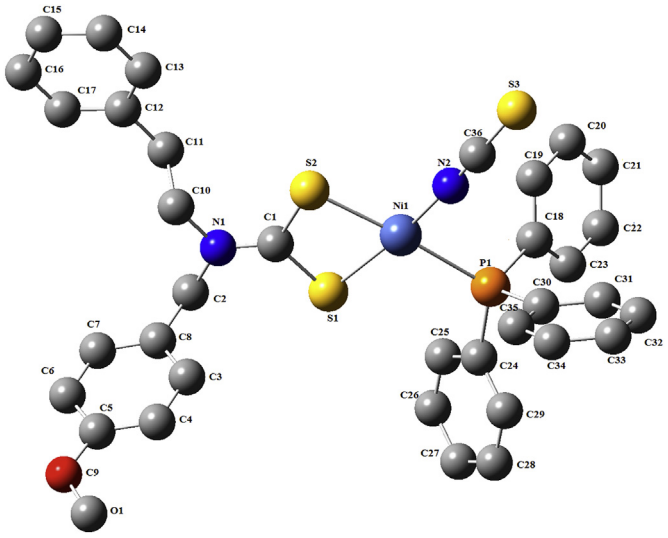

Fig. 11. Optimized structure of complex **10.**

The Ni–S distances [Ni–S1 = 2.2291(9), Ni–S2 = 2.1634(9) for **10**, Ni–S1 = 2.1702(10), Ni–S2 = 2.2245(9) for **12**] are asymmetric and Ni–P distance [2.1871(9) for **10** and 2.1903(8) for **12**] is short in the structures determined by X-ray crystallography. But in the optimized structure the Ni–S distances are symmetric and the Ni–P distance is longer [*ca.* 0.32]. These differences are also observed in related bond angles. These reveal that the *trans* influence and back bonding interaction between Ni and P are absent in gaseous state.

3.4.2.1. HOMO-LUMO. Frontier molecular orbital pictures of the optimized of the structure of the complexes **10** and **12** are shown in Fig. 13.The HOMO is located fully on sulfur and partially on nitrogen of NCS^- and the LUMO is more focused on the Ni (central metal atom) and phosphorous partially on C and N of NCS_2 group.

3.4.2.2. MEP. Molecular electrostatic potential (MEP) surface

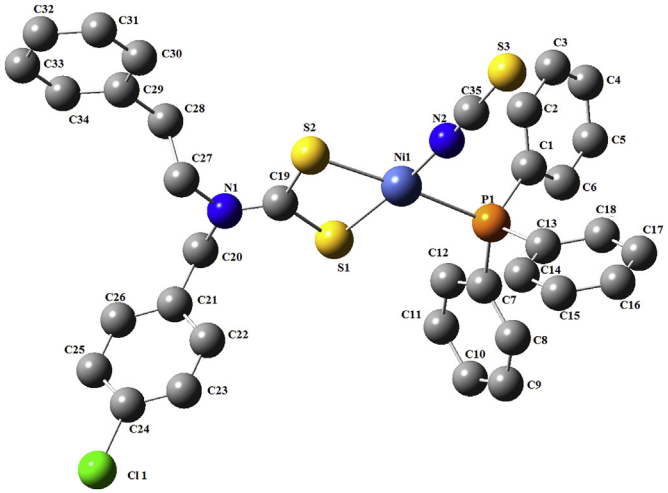

Fig. 12. Optimized structure of complex **12.**

Table 5
Comparison of selected optimized geometrical parameters of complexes **10** and **12** with experimental XRD parameters.

10				12			
Bond distances (Å)	XRD exptl.	Calcd	differences	Bond distances (Å)	XRD exptl.	Calcd	differences
Ni1–N2	1.866(3)	1.8991	0.0331	Ni1–N2	1.860(3)	1.8975	0.0375
Ni1–S2	2.1634(9)	2.3780	0.2146	Ni1–S1	2.1702(10)	2.3814	0.2112
Ni1–P1	2.1871(9)	2.5111	0.324	Ni1–P1	2.1903(8)	2.5079	0.3176
Ni1–S1	2.2291(9)	2.3969	0.1678	Ni1–S2	2.2245(9)	2.4005	0.176
S2–C1	1.726(3)	1.7955	0.0695	S1–C19	1.722(3)	1.7940	0.072
S1–C1	1.715(3)	1.7821	0.0671	S2–C19	1.708(3)	1.7796	0.0716
S3–C36	1.617(4)	1.6744	0.0574	S3–C36	1.620(4)	1.6738	0.0538
C36–N2	1.150(4)	1.1683	0.0183	C19–N1	1.318(4)	1.3158	0.0022
N1–C1	1.312(4)	1.3134	0.0014	C36–N2	1.150(4)	1.1685	0.0185
Bond angles (°)				Bond angles (°)			
N2–Ni1–S2	174.86(8)	172.80	2.06	N2–Ni1–S1	174.62(8)	172.66	1.96
N2–Ni1–P1	88.99(8)	89.49	0.5	N2–Ni1–P1	88.89(8)	89.64	0.75
S2–Ni1–P1	95.95(3)	97.60	1.65	S1–Ni1–P1	96.28(3)	97.62	1.34
N2–Ni1–S1	95.99(8)	95.96	0.03	N2–Ni1–S2	95.98(8)	95.90	0.08
S2–Ni1–S1	79.11(3)	76.97	2.14	S1–Ni1–S2	78.89(3)	76.84	2.05
P1–Ni1–S1	174.77(4)	174.41	0.36	P1–Ni1–S2	174.96(4)	174.40	0.56
C1–S2–Ni1	86.67(11)	85.49	1.18	C19–S1–Ni1	86.66(12)	85.44	1.22
C1–S1–Ni1	84.87(11)	85.21	0.34	C19–S2–Ni1	85.29(11)	85.18	0.11
N2–C36–S3	178.3(3)	179.01	0.71	N1–C19–S2	125.8(2)	123.87	1.93
N1–C1–S1	125.6(2)	123.94	1.66	N1–C19–S1	125.2(3)	123.60	1.6
N1–C1–S2	125.6(3)	123.74	1.86	S2–C19–S1	109.00(18)	112.52	3.52
S1–C1–S2	108.82(18)	112.31	3.49	N2–C36–S3	179.0(3)	179.01	0.01
C36–N2–Ni1	172.3(3)	174.53	2.23	C36–N2–Ni1	171.0(3)	174.62	3.62

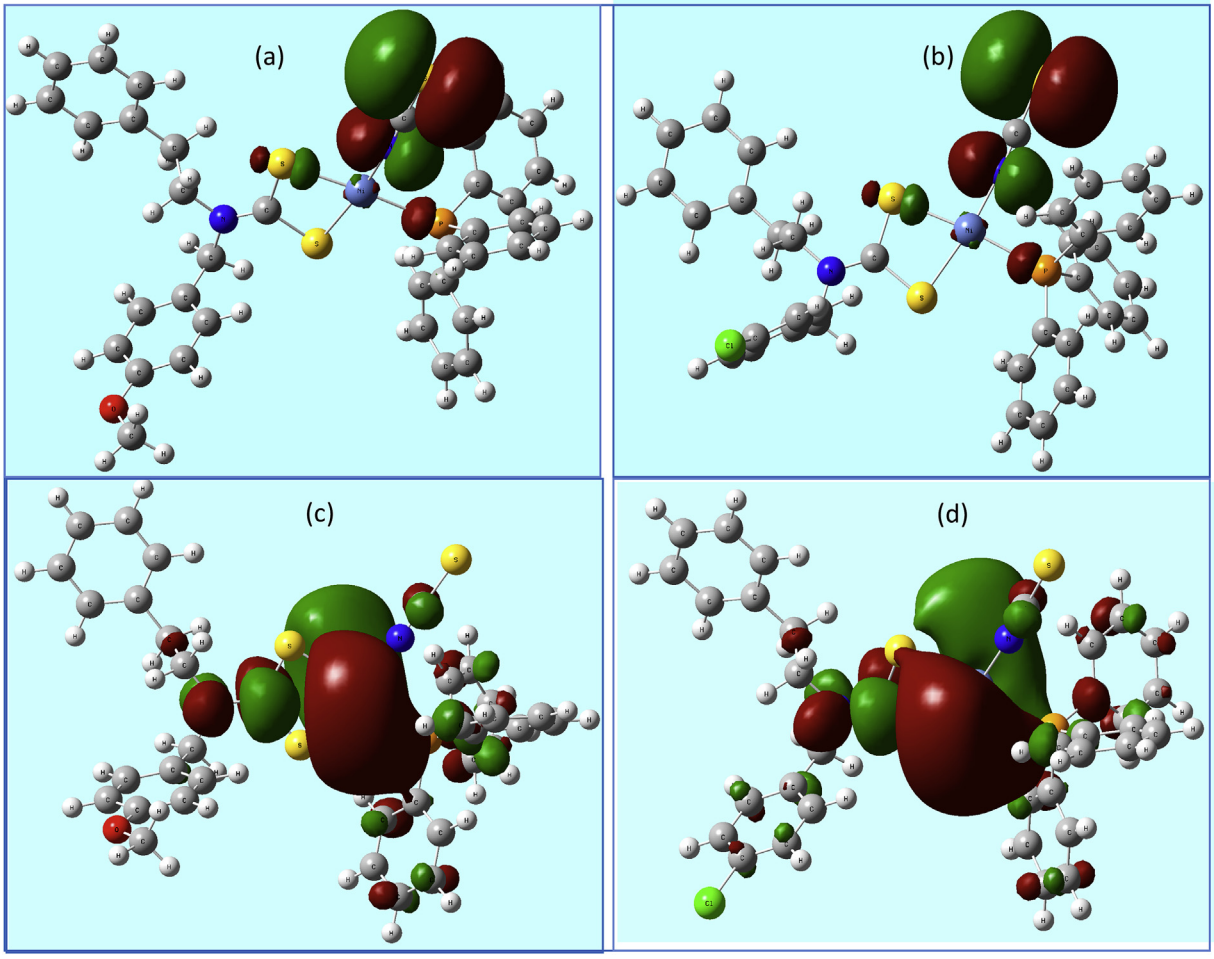

Fig. 13. The frontier molecular orbital (HOMO-LUMO) pictures of the optimized structures of **10** (a and c) and **12**(b and d).

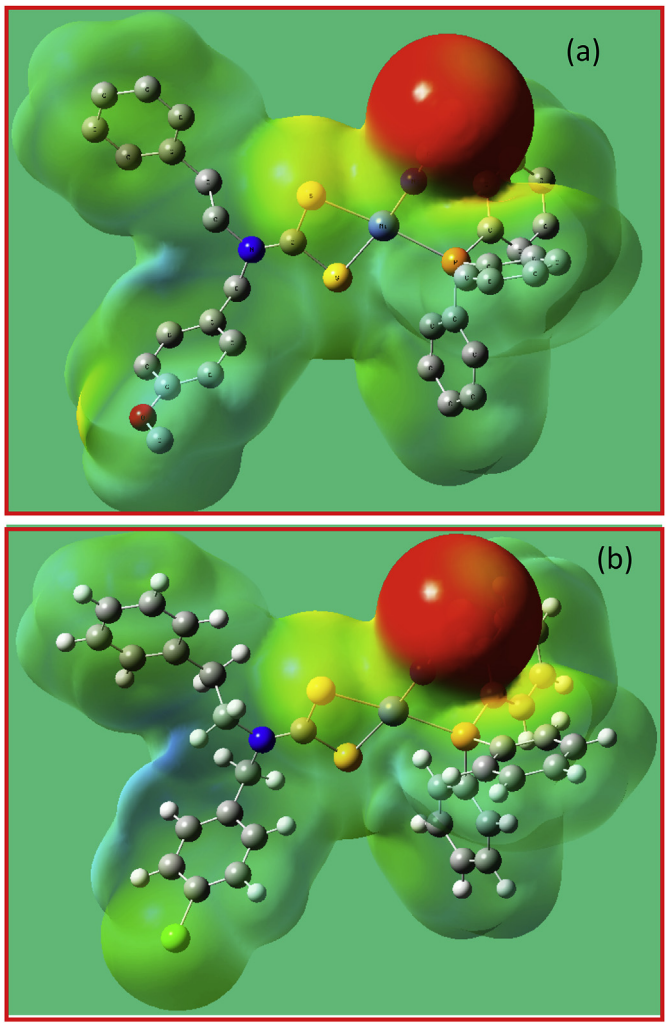

Fig. 14. Molecular electrostatic potential surface map of (a). **10** and (b). **12**.

diagrams (Fig. 14) provides a visual method to understand the relative polarity of a molecule. The negative electrostatic potential corresponds to an attraction of the proton by the concentrated electron density in the molecule (colored in shades of red), the positive electrostatic potential corresponds to repulsion of the proton by atomic nuclei in regions where low electron density exists and the nuclear charge is incompletely shielded (colored shades of blue). The different values of the electrostatic potential at the surface are represented by different colors; red represents regions of most electronegative electrostatic potential, blue represents regions of the most positive electrostatic potential and green represents region of zero potential. Potential increases in the order red < orange < yellow < green < blue [50,51]. MEP diagrams of complexes **10** and **12** reveal that the negative charge present on the sulfur atom of thiocyanate. The positive charge (blue) on the nitrogen atom and the negative charge (pale yellow) on the CS_2 moiety of dithiocarbamate ligands support the partial double bond character of C–N (thioureide) bond in dithiocarbamate moiety.

4. Conclusion

Twelve new homoleptic and heteroleptic Ni(II) complexes (**1**–**12**) with functionalized dithiocarbamate ligands have been prepared and characterized. Single crystal X-ray studies on **10** and **12** revealed the existence of intramolecular anagostic C–H···Ni interactions in both the complexes. This type of transition metal complexes with anagostic interaction may play important role in C–H activation in synthetic organic chemistry. Anagostic interaction is not observed in the optimized structures. This indicates that the packing effect is an important force to create the anagostic interaction. This study will be helpful in designing functionalized dithiocarbamate ligands containing a variety of substituents that may exhibit various interactions for their possible applications as novel functional materials.

Acknowledgment

The authors are thankful to Dr. SP. Meenakshisundaram, professor and former Head, Department of Chemistry, Annamalai University, Annamalainagar-608 002 for providing GAUSS IAN09 program.

Supplementary material

CCDC numbers **1431934** and **1431813** contain the supplementary crystallographic data for complexes **10** and **12**, respectively. These data can be obtained free of charge from the Cambridge Crystallographic Data Center via www.ccdc.cam.ac.uk/data_request/cif.

References

[1] M.C. Day, J. Selbin, Theoretical Inorganic Chemistry, second ed., 1969, p. 391.
[2] R.P. Burnsa, F.P.M.C. Colough, C.A. Auliffe, Adv. Inorg. Chem. radio Chem. 23 (1980) 211.
[3] A.R.K. Dapph, A. Ayame, Anal. Chim. acta 360 (1998) 43.
[4] E. Sathiyaraj, S. Thirumaran, Spectrochim. Acta A 97 (2012) 575.
[5] M.D. Regulacio, N. Tomson, S.L. Stoll, Chem. Mater. 17 (2005) 3114.
[6] N. Srinivasan, S. Thirumaran, Superlattices Microstruct. 51 (2012) 912.
[7] K. Ramasamy, M.A. Malik, P. O'Brien, J. Raftery, Dalton Trans. 39 (2010) 1460.
[8] B. Arul Prakasam, M. Lahtinen, A. Peuronen, M. Muruganandham, E. Kolehmainen, E. Haapaniemi, M. Sillanpaa, Polyhedron 81 (2014) 588.
[9] R. Chauhan, M. Trivedi, J. Singh, K.C. Molloy, G. Kociok-Kohn, U.P. Mulik, D.P. Amalnerkar, A. Kumar, Inorg. Chim. Acta. 415 (2014) 69.
[10] P. O'Brien, J. Waters, Chem. Vap. Depos. 12 (2006) 620.
[11] K. Ramasamy, W. Maneeprakorn, N. Iqbal, M.A. Malik, P. O'Brien, Int. J. Nanosci. 10 (2011) 815.
[12] T.A. Cottom, G. Wilkinson, Basic Inorganic Chemistry, John Wiley and Sons Inc., New York, 1962, p. 262.
[13] A. Nurmi, G. Goldsteins, J. Narvainen, R. Pihlaja, T. Ahtoniemi, O. Grohn, J. Koistinaho, Free Radic. Biol. Med. 40 (2006) 1776.
[14] P. Valarmathi, S. Thirumaran, L. Sarmal, R. Kant, Spectrochim. Acta Part A. 129 (2014) 285.
[15] P. Valarmathi, N. Srinivasan, S. Thirumaran, J. Sulfur Chem. 32 (2011) 583.
[16] E.R.T. Tiekink, J. Zukerman-Schpector (Eds.), The Importance of Pi-interactions in Crystal Engineering, John Wiley and Sons, 2012 (chapter 13).
[17] T. Steiner, Angew. Chem. Int. Ed. 41 (2002) 48.
[18] D.N. Sredojevic, Z.D. Tomic, S.D. Zaric, Cryst. Growth Des. 10 (2010) 3901.
[19] M. Nishio, Y. Umezawa, K. Honda, S. Tsuboyama, H. Suezawa, Cryst. Eng. Commun. 11 (2009) 1757.
[20] E.R.T. Tiekink, J.-Z. Schpector, Chem. Commun. 47 (2011) 6623.
[21] C.I. Yeo, S.N.A. Halim, S.W. Ng, S.L. Tan, J. Zukerman-Schpector, M.A.B. Ferreira, E.R.T. Tiekink, Chem. Commun. 50 (2014) 5984.
[22] A.N. Gupta, V. Kumar, V. Singh, K.K. Manar, M.G.B. Drew, N. Singh, Cryst. Eng. Commun. 16 (2014) 9299.
[23] B. Singh, M.G.B. Drew, G.K. Kohn, K.C. Molloy, N. Singh, Dalton Trans. 40 (2011) 623.
[24] V. Kumar, V. Singh, A.N. Gupta, K.K. Manar, L.B. Prasad, M.G.B. Drew, N. Singh, New J. Chem. 38 (2014) 3737.
[25] V. Singh, R. Chauhan, A.N. Gupta, V. Kumar, M.G.B. Drew, L. Bahadur, N. Singh, Dalton Trans. 43 (2014) 4752.
[26] V. Kumar, V. Singh, A.N. Gupta, K.K. Manar, M.G.B. Drew, N. Singh, CrystEngComm 16 (2014) 6765.
[27] T.S. Thakur, G.R. Desiraju, Chem. Commun. (2006) 552.
[28] J. Sabmannshausen, Dalton Trans. 41 (2012) 1919.
[29] T.R. Cook, Y.R. Zheng, P.J. Stang, Chem. Rev. 113 (2013) 734.
[30] R. Fu, S. Xiang, S. Hu, L. Wang, Y. Li, X. Huang, X. Wu, Chem. Commun. (2005) 5292.
[31] G.M. Sheldrick, Acta Crystallogr. A64 (2008) 112–122.
[32] G.M. Sheldrick, SHELXL-2013, University of Göttingen, Germany, 2013.

[33] D.C. Bradley, M.H. Gitlitz, J. Chem. Soc. A (1969) 1152.
[34] F. Bonati, R. Ugo, J. Organomet. Chem. 10 (1967) 257.
[35] P. Valarmathi, S. Thirumaran, L. Sarmal, R. Kant, Spectrochim. Acta, Part A 129 (2014) 285.
[36] P. Jamuna Rani, S. Thirumaran, Samuele Ciattini, Phosphorus Sulfur Silicon Relat. Elem. 188 (2013) 778.
[37] R. Baskaran, K. Ramalingam, G. Bocelli, A. Cantoni, C. Rizzoli, J. Coord. Chem. 61 (2008) 1710.
[38] S. Srinivasan, K. Ramalingam, C. Rizzoli, Polyhedron 33 (2012) 60.
[39] B. Arul Prakasam, M. Lahtinen, A. Peuronen, M. Muruganandham, E. Kolehmainen, E. Haapaniemi, M. Sillanpaa, Polyhedron 81 (2014) 588.
[40] N. Manav, A.K. Mishra, N.K. Kaushik, Spectrochim. Acta A 65 (2006) 32.
[41] S. Thirumaran, K. Ramalingam, Transit. Met. Chem. 25 (2000) 60.
[42] C.K. Jorgensen, J. Inorg. Nucl. Chem. 24 (1962) 1571.
[43] H.C.M. Van Gael, J.W. Diesveld, F.W. Pijpans, J.G.M. Van der Lin don, Inorg. Chem. 18 (1979) 3251.
[44] J.P. Fackler Jr., I.J.B. Lin, J. Andrews, Inorg. Chem. 16 (1977) 450.
[45] B. Arul Prakasam, K. Ramalingam, G. Bocelli, R.Z. Olla, Z. Anorg. Allg. Chem. 630 (2004) 301.
[46] L. Yang, D.R. Powell, R.P. Houser, Dalton Trans. (2007) 955.
[47] G. Hogarth, Prog. Inorg. Chem. 53 (2005) 71.
[48] G. Rajput, V. Singh, A.N. Gupta, M.K. Yadav, V. Kumar, S.K. Singh, A. Prashad, M.G.B. Drew, N. Singh, Cryst. Eng. Comm. 15 (2013) 4676.
[49] M.J. Frisch, G.W. Trucks, H.B. Schlegel, G.E. Scuseria, M.A. Robb, J.R. Cheeseman, G. Scalmani, V. Barone, B. Mennucci, G.A. Petersson, H. Nakatsuji, M. Caricato, X. Li, H.P. Hratchian, A.F. Izmaylov, J. Bloino, G. Zheng, J.L. Sonnenberg, M. Hada, M. Ehara, K. Toyota, R. Fukuda, J. Hasegawa, M. Ishida, T. Nakajima, Y. Honda, O. Kitao, H. Nakai, T. Vreven, J.A. Montgomery Jr., J.E. Peralta, F. Ogliaro, M. Bearpark, J.J. Heyd, E. Brothers, K.N. Kudin, V.N. Staroverov, R. Kobayashi, J. Normand, K. Raghavachari, A. Rendell, J.C. Burant, S.S. Iyengar, J. Tomasi, M. Cossi, N. Rega, J.M. Millam, M. Klene, J.E. Knox, J.B. Cross, V. Bakken, C. Adamo, J. Jaramillo, R. Gomperts, R.E. Stratmann, O. Yazyev, A.J. Austin, R. Cammi, C. Pomelli, J.W. Ochterski, R.L. Martin, K. Morokuma, V.G. Zakrzewski, G.A. Voth, P. Salvador, J.J. Dannenberg, S. Dapprich, A.D. Daniels, Ö. Farkas, J.B. Foresman, J.V. Ortiz, J. Cioslowski, D.J. Fox, Gaussian 09, Revision D.01, Gaussian Inc., Wallingford CT, 2009.
[50] S. Subashchandrabose, A.R. Krishnan, H. Saleem, S. Kavitha, V. Thanikachalam, G. Manikandan, J. Mol. Struct. 996 (2011) 1.
[51] M. Arockia doss, S. Savithiri, G. Rajarajan, V. Thanikachalam, C. Anbuselvan, Spectrochim. Acta A 151 (2015) 773.